

Supplementary Information

**Green and continuous route to assemble lateral nanodimensional
graphitic oxide composites without process interruption**

*Bijay Kumar Poudel,^a Kyung–Oh Doh^{*b} and Jeong Hoon Byeon^{*a}*

^aSchool of Mechanical Engineering, Yeungnam University, Gyeongsan 38541, Republic of Korea

^bDepartment of Physiology, Yeungnam University, Daegu 42415, Republic of Korea

*Corresponding authors: postjb@yu.ac.kr and kodoh@ynu.ac.kr

METHODS

- *Assembly of IDGO@DOX-PEG nanoflakes*

To prepare CEI nanoparticles first (**Fig. S1**), spark ablation (DC 3 kV, 2.2 mA) between graphite (C-072561, Nilaco, Japan) and iron (FE-222564, Nilaco, Japan) rods (3mm × 100mm) was employed under nitrogen gas (purity of 99.999%) flow (1.6 L min⁻¹). The specifications of the ablation were as follows: resistance, 0.5 MΩ; capacitance, 1.0 nF; loading current, 2.4 mA; and applied voltage, 3.4 kV. The spark-produced CEI particles were directly injected into K₂FeO₄ + H₂O₂ solution [CEI-10 mg, K₂FeO₄ (480010, Sigma-Aldrich, USA)-100 mg, DI water-10 mL, H₂O₂ (30 w/w% in H₂O, H1009, Sigma-Aldrich, USA)-20 mL) for IDGO assembly. The mass of CEI particles was measured using a piezobalance particle monitor (3522, Kanomax, Japan) in aerosol state. A gas tube for the injection was tangentially encountered to a cylindrical probe surface to apply ultrasound (20 kHz, 150 W, VCX-750, Sonics & Materials, USA) to generating nitrogen bubbles (containing the CEI particles). The solution was supplied via a peristaltic pump (323Du/MC4, Watson-Marlow Bredel Pump, USA) for 1 min 30 s of the ultrasound treatment. The ultrasound was employed both for oxidative exfoliation of graphitic layers from CEI particles and efficient decoration of iron nanoparticles on exfoliated GO nanoflakes subsequently to form IDGO nanoflakes. The solution was then sprayed out via the first atomizer as droplets to be injected into a denuder (a hollow tubular structure; inner section-flow path and outer section-mixture bed of silica gel and pelleted activated carbon) to remove the solution from the droplets. This IDGO nanoflake-laden nitrogen gas flow was employed as operating gas for spaying out (the second atomizer) DOX (0.1 g L⁻¹, 1225703, Sigma-Aldrich, USA)-PEG (0.1 g L⁻¹, 1546503, Sigma-Aldrich, USA) solution (cf. 0.8 g L⁻¹ for IDGO); thus, hybrid droplets containing IDGO, DOX, and PEG were sprayed out and subsequently injected into a heated tubular reactor (90°C wall temperature, 12 s residence time) to extract solvent from the hybrid droplets to form IDGO@DOX-PEG nanoflakes. The identical lab-made atomizers containing a 0.3 mm orifice were adopted to this process, and the flow rate and pressure of nitrogen gas (<10⁻¹ impurities) were 1.0 L min⁻¹ and 0.3 MPa, respectively. The

nanoflakes were electrostatically collected in a single-pass configuration on a polished aluminum rod (2.7 kV cm^{-1}) in powder formulation. These powders were dispersed in PBS (0.01 M, pH 7.4, 806552, Sigma-Aldrich, USA) just before the bioassays.

- ***Characterizations***

1) Size distribution in aerosol state

The size distribution of fabricated IDGO, IDGO@DOX, IDGO@DOX-PEG flakes, including individual iron, graphitic carbon, and CEI nanoparticles were determined using SMPS (3936, TSI, USA). The flow rates of sampling and sheathing for SMPS measurements were 0.1 and 1.0 L min^{-1} , respectively, and the scan time was 135 s.

2) Morphological analysis

The assembled nanoflakes were directly collected on a carbon-coated copper grid (Tedpella, USA) via TEM grid filtration (Ineris, France) in a gaseous single-pass configuration (0.2 L min^{-1} flow rate) with no pre- and post-treatments. The iron, graphitic carbon, and CEI nanoparticles were also collected on another grid for comparison purposes. The specimen was prepared for examination in the STM by direct electrostatic aerosol sampling at a sampling flow of 0.2 L min^{-1} and an operating voltage of 3 kV using a nano particle collector (NPC-10, HCT, Korea). The TEM grid filtration and electrostatic sampling employed direct suction of the gas flow using a vacuum pump (3033, TSI, USA) right after the denuder. The grid was transferred to a holder for TEM analyses (G2 F20 S-TWIN, Tecnai, USA) at increasing voltages in the range of 50–300 kV. The IDGO@DOX-PEG nanoflakes were deposited on mica plates (Ted Pella, Inc., USA) and viewed under STM (Nanoscope®IIIa ECSTM, Digital Instruments, USA). The constant height mode was employed with platinum-iridium tips (0.25 mm diameter, Veeco Inc., USA) to acquire images. The STM measurements were performed at ambient condition with a scan rate of 20.3 Hz and a stabilization voltage and current of 100 mV and 65 pA, respectively.

3) Surface chemistry and light absorption

Difference in the surface chemistry between the IDGO and IDGO@DOX-PEG (or IDGO@DOX) flakes was evaluated using FTIR (iS-10, Thermo Electron, USA) in absorbance mode ($1300\text{--}3300 \text{ cm}^{-1}$)

consisting of a highly sensitive mercury cadmium telluride (MCT) detector after nanoflake deposition onto a polytetrafluoroethylene (PTFE) substrate (11807-47-N, Sartorius, Germany). The specimens for FTIR measurements were prepared on glass discs (260377, TedPella, USA) placed on PTFE substrates. The disc/PTFE was placed on a sampling plate of a nano particle collector (NPC-10, HCT, Korea) with a sampling flow of 0.2 L min⁻¹ and an operating voltage of 3 kV. The disc was then detached and used for the measurements with 32 scans. The composition of IDGO@DOX-PEG flakes was confirmed using XPS (Axis-HIS, Kratos Analytical, Japan).

The light absorption spectra of nanoflakes dispersed in PBS were measured using UV-vis spectroscopy (T60, PG Instruments, UK). The Raman spectra of IDGO flakes, including graphitic carbon and CEI nanoparticles were detected using Raman spectroscopy (XploRA Plus, Horiba, Japan).

4) Thermogravimetric analysis

TGA curves of CEI and IDGO were achieved using a PerkinElmer Diamond TG/DTA instrument under nitrogen from room temperature to 800°C (10°C min⁻¹).

5) Magneto- and photo-thermal activity

The magneto- and photo-thermal effects were tested in the IDGO nanoflake dispersed PBS at the chosen concentrations (1 mg mL⁻¹ for magneto-thermal; 100 µg mL⁻¹ for photo-thermal) The induction heating ability of IDGO was evaluated under the applied field strength (H_0) of 60 kAm m⁻¹) and frequency of 200 KHz. In the case of photothermal heating, IDGO was exposed to 808 nm NIR laser irradiation (FC-W-808 nm-30W, Changchun New Industries Optoelectronics Technology, China) with power density of 2.5 W cm⁻². Increased temperatures for the magneto- and photo-irradiation were measured using an IR thermometer (572-2, Fluke, USA) and a high resolution IR camera (Therm-App TH, Opgal Optronic Industries Ltd, Israel), respectively.

6) DOX release

In vitro cumulative release of DOX from DOX-PEG and IDGO@DOX-PEG nanoflakes was assessed in ABS (pH 5.8) and PBS (pH 7.4). 1 mL of nanoflakes dispersion was placed in a dialysis bag (MWCO: 3500 Da, Spectra/Por®, USA), clipped at the both sides and immersed into a 50 mL tube

containing 30 mL of ABS or PBS. The tube was then dipped in a water bath shaker (HST-205 SW, Hanbaek ST Co., Korea) at 100 strokes per min at a temperature of 37°C. Certain volume of media aliquots were withdrawn at predetermined time interval and replaced with equal volumes of fresh media maintained at 37°C. The cumulative amount of DOX released was determined by UV-vis spectrophotometry (U-2800, PerkinElmer, Japan).

7) Vibrating sample magnetometry

The IDGO@DOX-PEG nanoflakes were placed in a vibrating sample magnetometer (7404, Lake Shore Cryotronics, USA) to characterize the magnetic properties at 300K.

- Biological assays

All biological assays were performed in HeLa cells. HeLa cells were grown in RPMI-1640 (HyClone, GE Healthcare Biosciences, USA) supplemented with 10% heat-inactivated FBS and antibiotics (100 units mL⁻¹ penicillin, 100 µg mL⁻¹ streptomycin, and 250 ng mL⁻¹ amphotericin B). Cultures are incubated at 37°C, 5% CO₂-humidified incubation chamber, and passaged regularly when confluence reached 70–80%.

1) Cytotoxicity

Cytotoxicity measurements for IDGO@DOX and IDGO@DOX-PEG nanoflakes, including free DOX and IDGO nanoflakes in the absence and presence of magneto- or photo-irradiation were measured in HeLa cells via MTT assay after 48-h incubation. Briefly, 1 × 10⁴ cells (HeLa, L929, and HNEpC) per well were plated into 96-well microtiter plates (Becton Dickinson Labware, USA) and incubated for 12 h for cell attachment. After 48 h, the cells were washed, and 100 µL MTT solution (1.25 mg mL⁻¹) was added into each well. During a 4 h incubation in the dark, live cells produced violet-colored formazan crystals as a product of MTT metabolism. The crystals were dissolved in 100 µL DMSO, and the absorbance was measured at 570 nm using a microplate reader (Multiskan EX, Thermo Scientific, USA). Cell viability was calculated as $A_{\text{sample}}/A_{\text{control}} \times 100\%$, where A is the absorbance at 570 nm.

2) Cellular uptake

For cellular internalization study by fluorescent microscopy, 2 mL of HeLa cells (10^5 cells) were plated in a 12-well plate. After 12 h incubation, the DOX-PEG and IDGO@DOX-PEG were added and incubated for 24 h. The cells were washed with PBS and co-stained with TO-PRO-3 dye in PBS to the final concentrations of 2 μ M, and were then observed using inverted fluorescence microscopy (Eclipse Ti, Nikon, Japan)

For quantitative cellular internalization study by FACS, 2 mL of medium containing HeLa cells (5×10^4 cells mL^{-1}) were seeded in 12-well plates, and incubated overnight. The cells were then treated with DOX-PEG and IDGO@DOX-PEG nanoflakes, and incubated for 2 h and 6 h, respectively. After incubation, the cells were washed with PBS, trypsinized, and harvested. The cells were then dispersed in 1 mL of PBS containing binding buffer for flow cytometric analysis using an FACS flow cytometer (BD Biosciences, USA). Auto-fluorescence of untreated cells was used as an internal control.

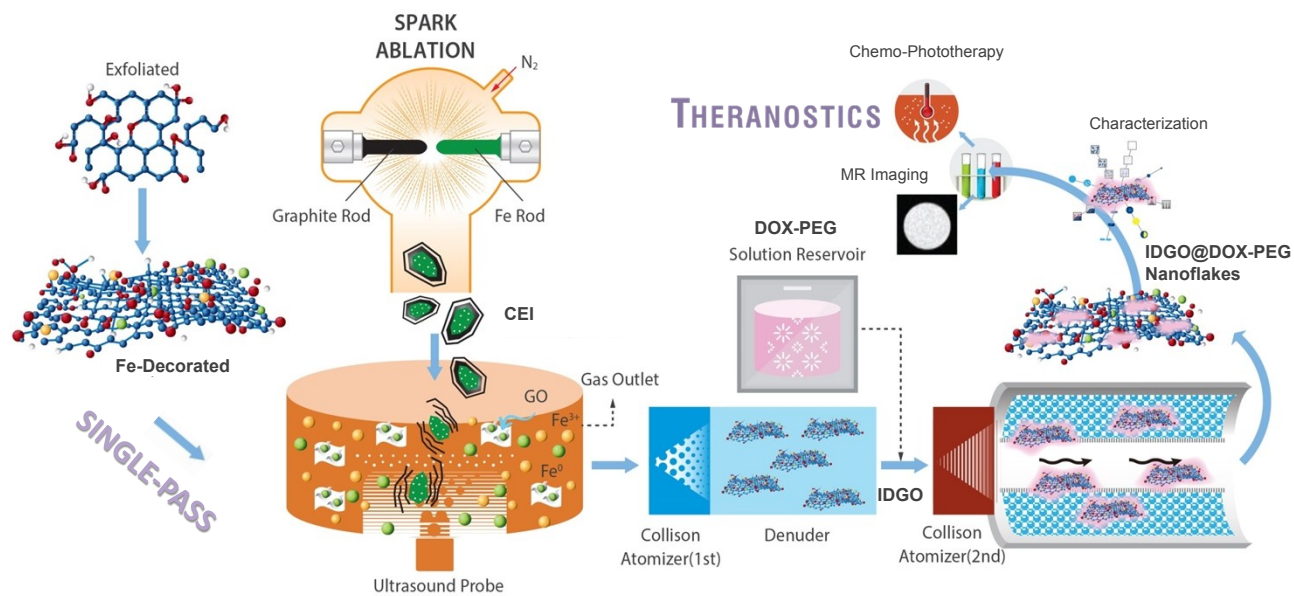
3) Live/dead assay

HeLa cells were seeded in a 6-well plate (1×10^5 cells per well) and incubated for 24 h. IDGO@DOX-PEG nanoflakes were added and incubated for 3 h at 37°C. After washing the cells, the plate was placed under approximately 2 mm of laser beam ($\lambda = 808$ nm, 2.5 W cm^{-2}) diameter for 2 min. The cells were then washed, replenished with fresh Dulbecco's modified Eagle medium, and incubated for 3 h. The plates were observed using inverted-fluorescence microscopy (Eclipse Ti, Nikon, Japan) after the cells were stained with 5 μ L of calcein-AM (live cells) and ethidium homodimer-1 (EthD-1, dead cells).

4) MR imaging

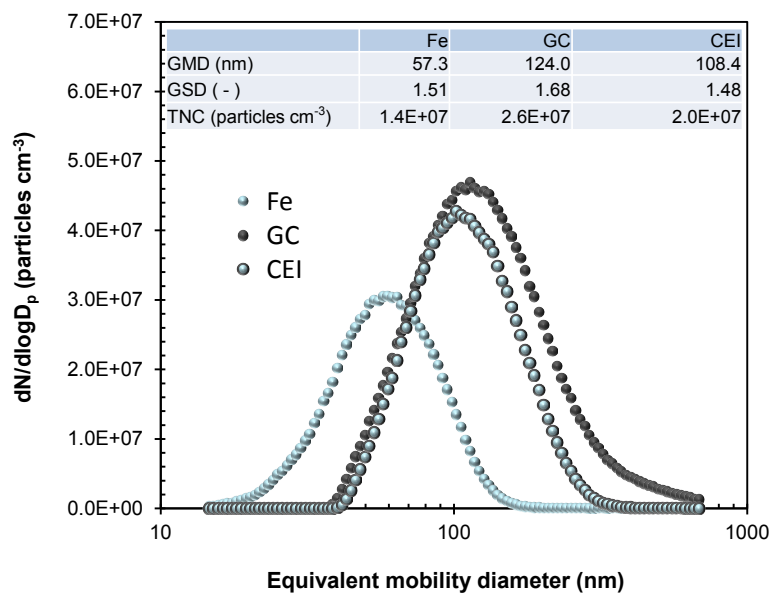
For *in vitro* MR imaging, 5×10^4 cells per well were plated, and incubated for 24 h. The calculated amount of IDGO@DOX-PEG corresponding to Fe concentration of 5, 10, 15 and 20 $\mu\text{g mL}^{-1}$ were added, and incubated at 37°C for 3 h. The cells were then washed with PBS, harvested, centrifuged, and resuspended in 0.3 mL of 2% agar at approximately 60°C. The samples were quickly transferred to a 96-well plate to allow the suspensions to solidify for MR imaging. MR images are acquired on 3.0-T preclinical MR scanner (Achieva 3.0T TX, Philips, Netherlands).

FIG. S1



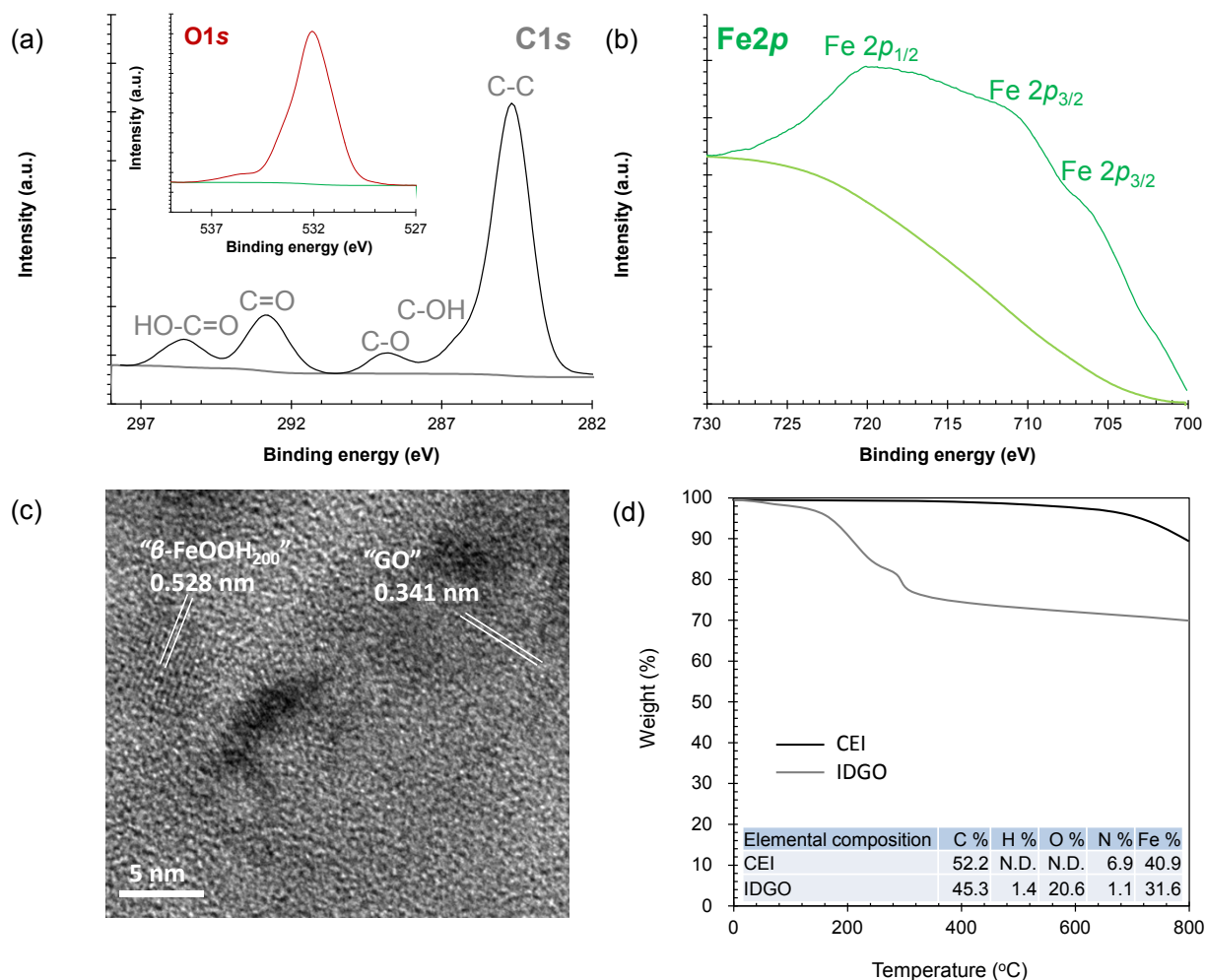
Detailed schematic of IDGO@DOX-PEG nanoflake assembly. The precursors of iron nanoparticles and GO in IDGO were supplied via spark ablation between iron and graphite rods under nitrogen gas flow. A catalytic graphitization on molten iron during co-condensation of ablated iron and carbon under nitrogen gas flow induced the formation of CEI nanoparticle that contains metallic iron core with several graphitic layers. The CEI nanoparticles were then injected into the exfoliation solution under ultrasound irradiation before the orifice of the first Collision atomizer. Eventually, the IDGO nanoflakes were incorporated with DOX-PEG at the second atomizer and thermally dried to form IDGO@DOX-PEG nanoflakes in a single-pass configuration. The nanoflakes were electrostatically collected (+ field) in an aerosol state and dispersed in PBS for *in vitro* bioassays.

FIG. S2



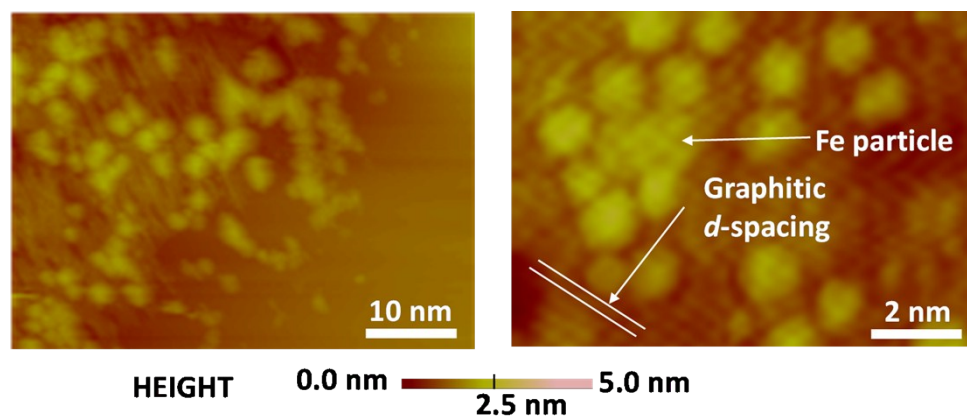
Size distributions of CEI nanoparticles, including iron (Fe) and graphitic carbon (GC) nanoparticles before injecting into exfoliation solution. Summaries (GMD, GSD, and TNC) of the distributions are also displayed as inset.

FIG. S3



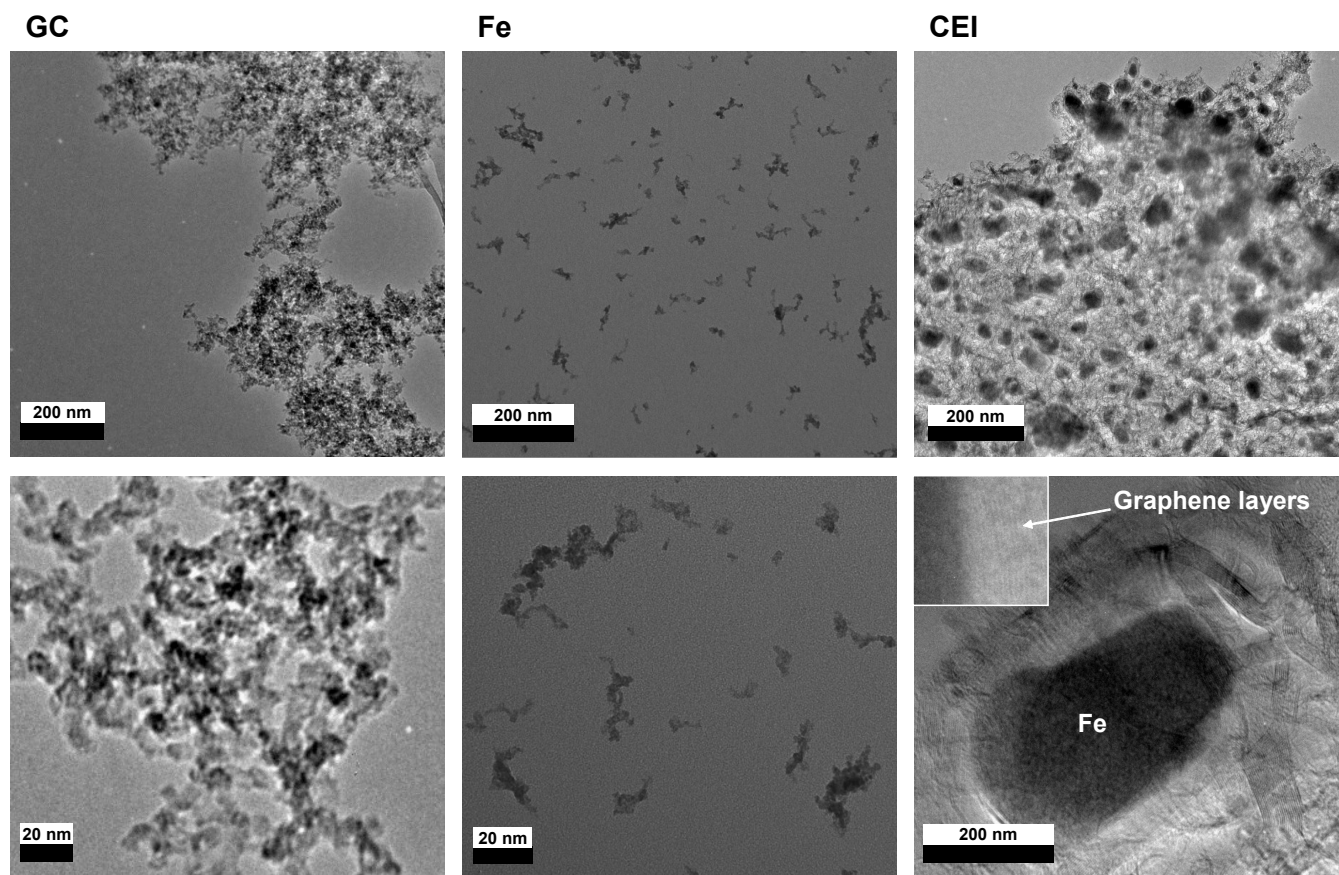
C1s and Fe2p XPS spectra of IDGO flakes. (a) C1s XPS spectrum after the ultrasonic reaction of CEI nanoparticles. Peaks corresponding to oxidized carbons demonstrate the formation of GO flakes (also refer to O1s spectrum, inset) from CEI particles. (b) A peak at 706.6 eV corresponds to 2p_{3/2} of zero-valent iron (Fe⁰) confirms the presence of metallic iron. The spectrum also shows asymmetric peaks at binding energies of 719.7 eV and 710.3 eV respectively corresponding to Fe 2p_{3/2} and Fe 2p_{1/2} electronic configuration of iron hydroxide (FeOOH) with a splitting of 9.4 eV. This implies that the decorated particles on GO flakes were not iron oxide nanoparticles (i.e., hematite or magnetite). (c) High-magnification TEM image of IDGO flake containing a β -FeOOH particle on an GO. This result supports the XPS spectrum, which shows existence of FeOOH particles on GO surfaces. (d) TGA curves and elemental compositions of CEI and IDGO samples.

FIG. S4



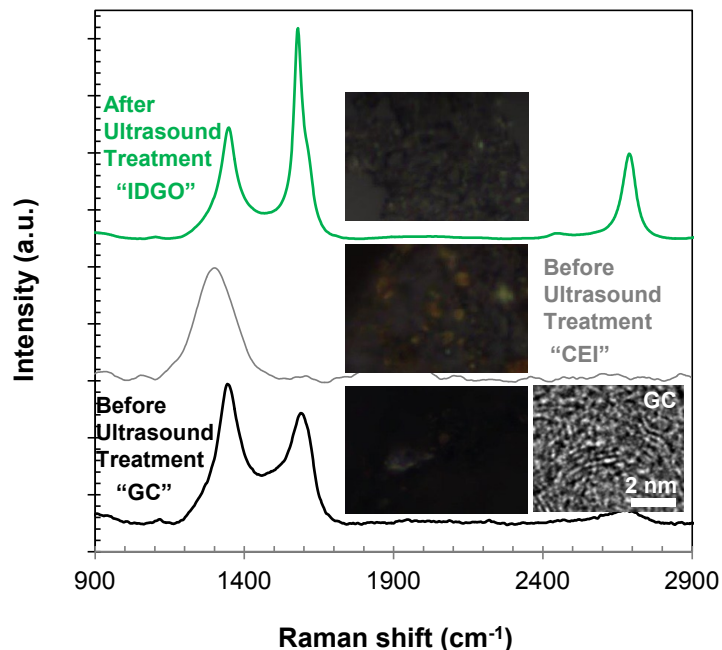
Representative STM images of IDGO flakes. Approximately 1 nm and 3 nm thicknesses were detected for individual graphitic and Fe deposited graphitic layers, respectively, proving restructuring of Fe cores and graphitic shells from CEI particles.

FIG. S5



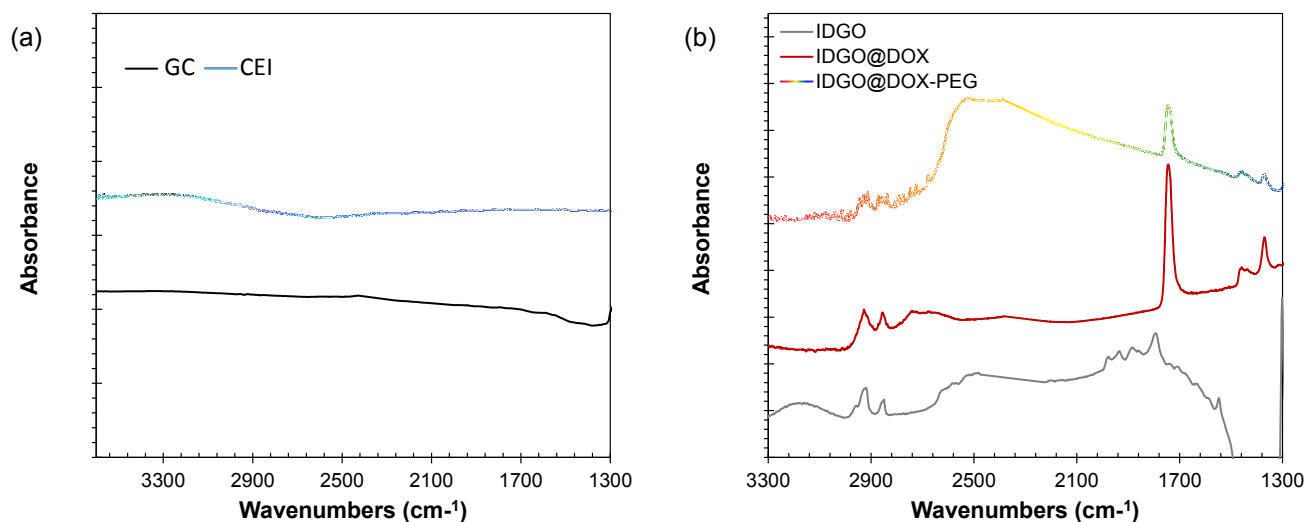
Low- and high-magnification TEM images of graphitic carbon (GC), iron (Fe), and CEI nanoparticles. A high-magnification TEM image (inset of CEI) shows graphitic layers on an iron core particle. Even though the homogeneous spark ablation between identical graphite (or iron) rods produced agglomerated structures, the catalytic graphitization on iron particles induced transformation of carbon, resulting in the formation of multiple graphitic layers.

FIG. S6



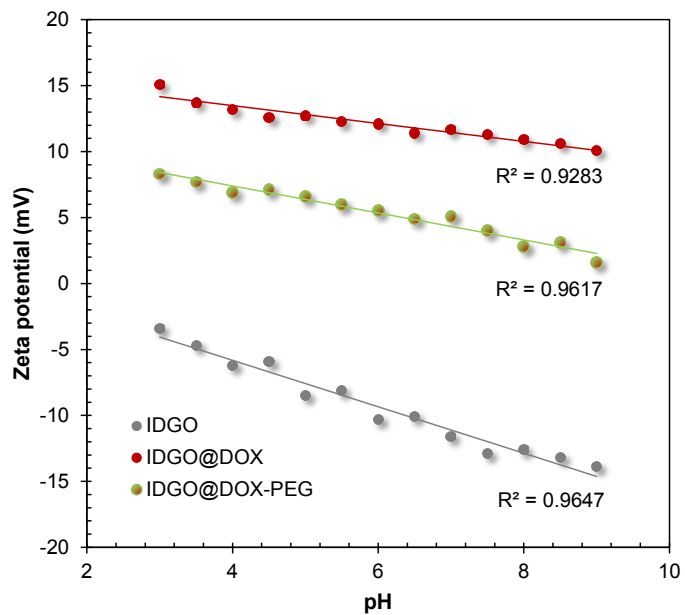
Raman spectra of the IDGO nanoflakes, including GC and CEI nanoparticles. Optical microscope images of the samples on glass discs are also shown as insets. Even though graphitic structures (*D*–*G* doublets) of the GC particles were not found in CEI particles (i.e., carbonaceous stretching modes at around 1280 cm^{-1} in fullerene-like carbons), peaks in the region $1200\text{--}1700\text{ cm}^{-1}$ could clearly be seen for IDGO flakes. Colors and shapes (insets) due to light reflecting from the different structures (GC, CEI, and IDGO) correspond to the Raman spectra. A high-magnification TEM image of GC particles (another inset) exhibited a similar microstructure to that of amorphous carbon or activated charcoal.

FIG. S7



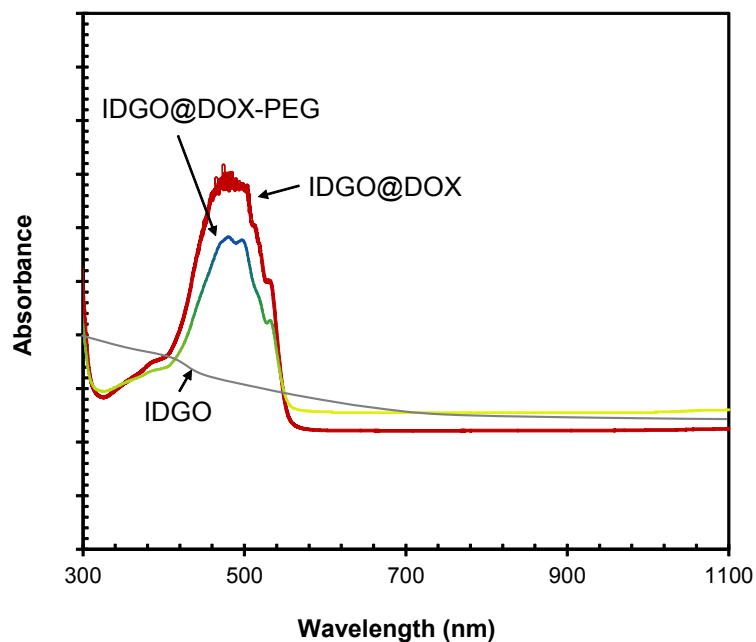
FTIR spectra of samples (a) before and (b) after ultrasonic exfoliation. Featureless spectra were shown in GC and CEI particles (a), implying that those particles did not contain oxidized carbons (i.e., common graphitic structures are existed similar to graphenes or reduced graphene oxides.). IDGO shows broad IR peaks at around 3200 and 1700 cm^{-1} corresponding to the O–H stretching and C=C vibrations, respectively, and also shows CH bend (around 2950 cm^{-1}) and carboxyl C=O (around 1800 cm^{-1}). C–O bending (1400 cm^{-1}) and C=O stretching (1740 cm^{-1}) in carboxyl groups as molecular bone of DOX are clearly seen in spectra of DOX incorporated samples (IDGO@DOX and IDGO@DOX-PEG), supporting conjugation between the IDGO and DOX during the assembly. The superimposition of the PEG induced changes in absorbance at 2950, 1740, and 1400 cm^{-1} , as well as produced a shoulder at around 2600 cm^{-1} .

FIG. S8



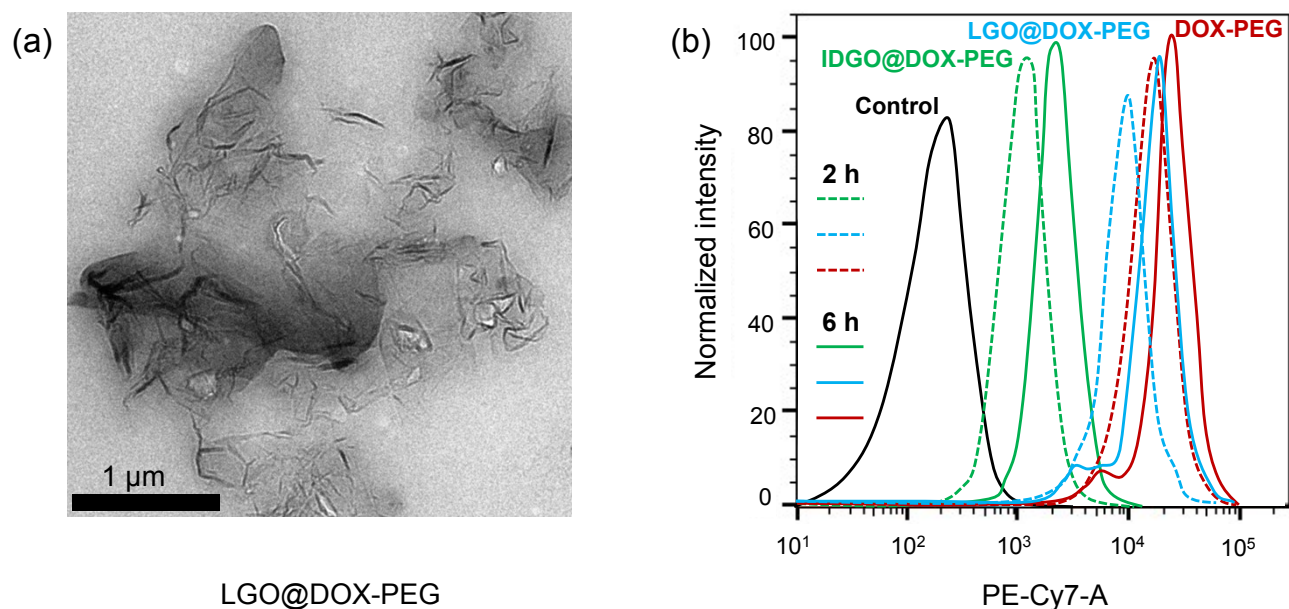
Zeta potentials of IDGO@DOX-PEG flakes, including IDGO and IDGO@DOX flakes. The values depended on pH of media (i.e., PBS), and the negative surface charges of IDGO flakes shifted to positive polarity in DOX incorporated samples because of amine groups in DOX. The PEG incorporation further changed surface charges of IDGO flakes, and this implies that the proposed assembly was suitable to conjugate DOX and PEG on IDGO flakes.

FIG. S9



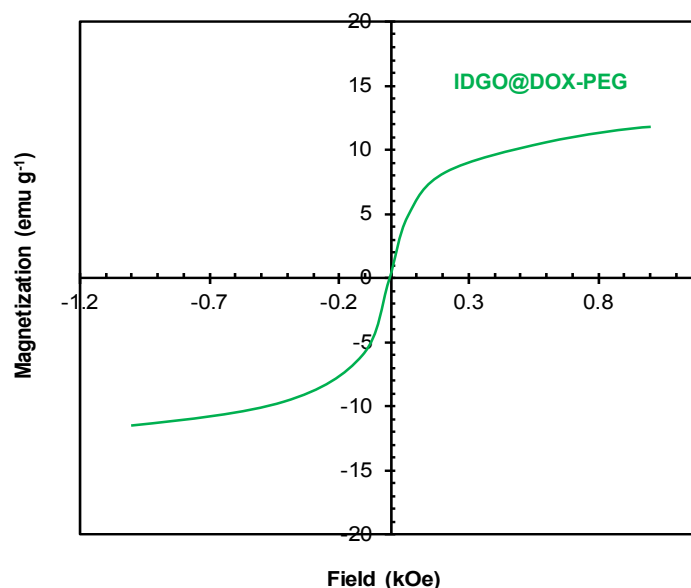
UV-vis spectra of IDGO@DOX-PEG flakes, including IDGO and IDGO@DOX flakes. Absorbances of DOX are clearly introduced in IDGO@DOX and IDGO@DOX-PEG flakes, supporting incorporation of the GO and DOX during the assembly. This implies that the second atomization was feasible for adding both DOX and DOX-PEG without further treatments.

FIG. S10



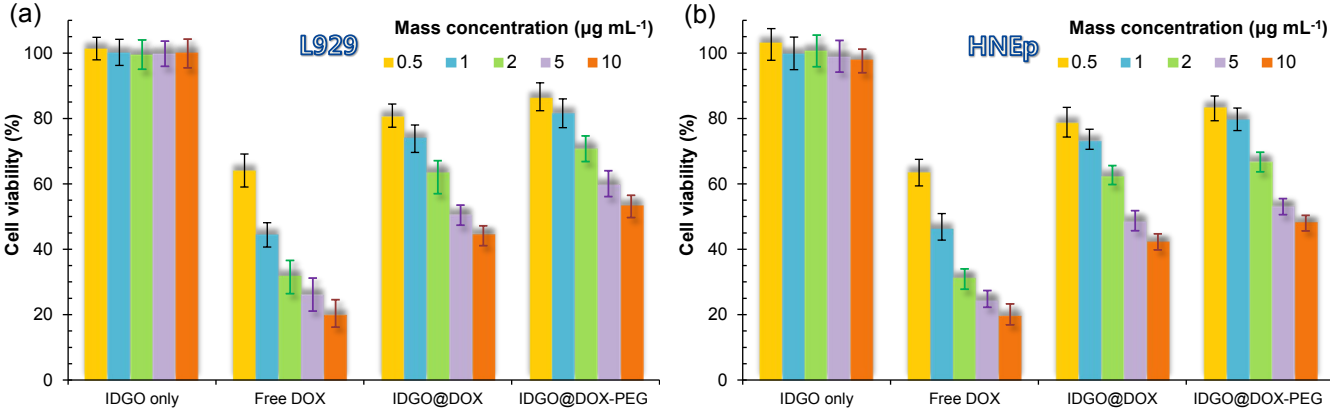
Comparison in controlled DOX release between IDGO@DOX-PEG and large (lateral microdimensional) GO@DOX-PEG (i.e., LGO@DOX-PEG) flakes. (a) TEM image of LGO@DOX-PEG flakes. (b) FACS analyses of IDGO@DOX-PEG and LGO@DOX-PEG flakes, including DOX-PEG by HeLa cells following 2 and 6 h incubation. The suppression of burst DOX release for LGO@DOX-PEG flakes is weaker than that for IDGO@DOX-PEG, implying that the larger amount of surfaces and edges in IDGO nanoflakes for DOX conjugation enhanced the controlled DOX release activity.

FIG. S11



Magnetization profile of IDGO@DOX-PEG flakes at 300 K. The result shows the absence of coercive hysteresis for IDGO@DOX-PEG flakes indicating that the IDGO conserves superparamagnetic behavior [saturation magnetization (M_s) value is 11.8 emu g^{-1}] after incorporation with DOX-PEG. The observed M_s of the flakes is lower than the pure iron nanoparticles, because passivation of iron nanoparticles via GO crumpling and DOX-PEG conjugation that are diamagnetic materials, therefore interparticle coupling between the components probably decreases the magnetic property. The FeOOH particles instead of pure iron also decrease the magnetization.

FIG. S12



In vitro cytotoxicities of IDGO@DOX and IDGO@DOX-PEG flakes, including IDGO and free DOX against (a) L929 and (b) HNEp cells ($p < 0.05$).